Pure Appl. Chem., Vol. 80, No. 11, pp. 2521–2536, 2008.
doi:10.1351/pac200880112521

Synthesis and electrochemical studies on surface-modified $LiCoVO_4$ with La_2O_3 and malonic acid for cathode material of Li-ion cells*

George Ting-Kuo Fey‡, Yung-Da Cho, and Pandurangan Muralidharan

Department of Chemical and Materials Engineering, National Central University, Chung-Li, Taiwan 32054 R.O.C.

Abstract: An inverse spinel $LiCoVO_4$ cathode material was synthesized by a citric acid-urea polymeric method, calcined at 773 K for 5 h. The synthesized $LiCoVO_4$ sample was surface-modified with La_2O_3 and/or malonic acid. The composite materials were comprehensively characterized with the aid of various spectroscopic and analytical techniques. X-ray diffraction (XRD) patterns revealed that single-phase crystallinity occurred when they were heated at 773 K for 5 h in air. For the La_2O_3-coated samples, there was no evident signal corresponding to secondary-phase peaks. Fourier transform infrared (FTIR) spectra showed the complete elimination of organic residues, nitrates, and the formation of pure $LiCoVO_4$ at 773 K. The two strong peaks due to sp^2 and sp^3 carbon bonding in the Raman spectra clearly confirm the presence of carbon coating at the surface of $LiCoVO_4$ particles. Transmission electron microscopy (TEM) images showed that the 0.5 wt % La_2O_3-coated $LiCoVO_4$ material calcined with 60 wt % malonic acid was compact with an average thickness of about 15 nm. This composite cathode material also demonstrated the best cell performance with an initial capacity of 71 $mAhg^{-1}$ and better thermal stability with lower heat evolution of 35 Jg^{-1}, and a higher onset temperature of thermal decomposition at 475 K, vs. 176 Jg^{-1} and 452 K for the bare $LiCoVO_4$ sample.

Keywords: citric acid-urea; La_2O_3; $LiCoVO_4$; Li-ion cells; surface modification.

INTRODUCTION

Since the discovery of both $LiNiVO_4$ and $LiCoVO_4$ as new cathode materials for secondary Li batteries in 1993 [1], interest in inverse spinel materials has arisen due to their high-voltage behavior. A family of inverse spinel vanadate cathode materials such as $LiCoVO_4$ (4.3 V), $LiNi_yCo_{1-y}VO_4$ (y = 0.1–0.9) and $LiNiVO_4$ (4.8 V) were investigated by Fey et al. [2–11]. In this structure, Li^+ ions reside in octahedral sites and Co^{2+} and Ni^{2+} ions and V^{5+} ions were distributed both in octahedrally and tetrahedrally coordinated sites.

Many attempts have been made to enhance the electrochemical properties of $LiNiVO_4$ and $LiCoVO_4$ materials through different synthesis techniques, such as the glycine-nitrate combustion

*Paper based on a presentation at the 3rd International Symposium on Novel Materials and Their Synthesis (NMS-III) and the 17th International Symposium on Fine Chemistry and Functional Polymers (FCFP-XVII), 17–21 October 2007, Shanghai, China. Other presentations are published in this issue, pp. 2231–2563.

‡Corresponding author: Tel./Fax: +886-3-425-7325; E-mail: gfey@cc.ncu.edu.tw

process [12], citric complex method [13], and starch-assisted combustion process [14]. The particle sizes of powders synthesized by these methods are normally in the micrometer range. Vivekanandhan et al. [15] synthesized crystalline 39-nm $LiNiVO_4$ by using a 1:1 ratio of metal ions to glycerol. Thongtem et al. [16] also successfully prepared nanocrystalline 31-nm $LiCoVO_4$ by a solvothermal reaction at 423 K and subsequent calcination at 573 K. Landschoot et al. [17] synthesized Fe-doped $LiCoVO_4$ with Al_2O_3 coating by the citric complex method, and showed that the first discharge capacity was 76 $mAhg^{-1}$ with good capacity retention due to the ability of the Al_2O_3 layer to neutralize the HF component in the liquid electrolyte. Recently, Fey et al. [18] synthesized Al_2O_3-coated $LiCoVO_4$ by a polymeric process, and reported that the 0.5 wt % Al_2O_3-coated $LiCoVO_4$ delivered an initial discharge capacity of 68 mAh g^{-1}. The Al_2O_3 coating technique was also applied to another inverse spinel materials of $LiNiVO_4$ [19].

The major limitations associated with the inverse spinel vanadates were low discharge capacities with respect to their theoretical capacity (148 $mAhg^{-1}$), initial drastic drops in capacity and large capacity fades during continuous cycling [1,3,7,9,11]. These problems may be related to various factors, such as low electronic conductivity [6], cobalt dissolution into the HF-containing electrolyte in the case of cobalt-based cathodes [20,21], and a disproportionate reaction at the surface of the cathode materials resulting in structural changes of the host material [22]. The very high cell voltage of 4.8 V obtained using $LiNiVO_4$ as a cathode has not been advantageous, because most electrolytes can be oxidized by the cathode material at voltages higher than 4.5 V [11,23], leading to a significant deterioration in cycle performance [24,25]. However, the $LiCoVO_4$ cathode exhibits 4.2 V, which is more suitable for some oxidation-resistant electrolytes. Furthermore, the weight percentages of cobalt in $LiCoVO_4$ and $LiCoO_2$ are 32.6 and 60.2, respectively. The lower weight percentage of cobalt in $LiCoVO_4$ does not have an immediately obvious cost advantage over $LiCoO_2$, since there are differences in capacity. In the case of $LiCoO_2$, it is 140 $mAhg^{-1}$, and in the case of $LiCoVO_4$, it is 71 $mAhg^{-1}$. The cost advantage of $LiCoVO_4$ only becomes significant when its capacity is greatly increased.

Recently, $LiFePO_4$ has emerged as a new high-power cathode material for large-size Li-ion batteries in applications related to power tools, electric vehicles (EVs), and hybrid electric vehicles (HEVs). This rapid advancement in high rate capability was achieved by significantly improving electronic conductivity and Li^+ diffusion kinetics through the use of non-lattice doping with carbon [26–30] and lattice doping with supervalent elements [31–35]. The bare $LiFePO_4$ sample without carbon coating or metal doping shows very low initial capacity and poor electronic conductivity. Both pristine $LiNiVO_4$ and $LiCoVO_4$ samples display similar behavior of low capacity and conductivity. Therefore, we attempt to adopt a similar $LiFePO_4$ approach to improve the $LiCoVO_4$ cathode system.

To obtain higher capacities and decrease the capacity fades, in this work, we prepared the pristine $LiCoVO_4$ powder and La_2O_3-coated $LiCoVO_4$ materials by a citric acid-urea polymeric method, and La_2O_3-coated $LiCoVO_4$/carbon composite cathode materials by a solid-state high-temperature method. The prepared samples were characterized by various techniques and their cell performance and coating effect was evaluated in terms of discharge capacity, cycle life, and thermal stability.

EXPERIMENTAL

Synthesis of $LiCoVO_4$

According to the stoichiometric composition, proper amounts of $LiNO_3$, $Co(NO_3)_2{\cdot}6H_2O$ (Merck, >99 %), and NH_4VO_3 (Acros Organics, >98 %) to obtain $LiCoVO_4$ were dissolved in deionized water under constant magnetic stirring at 353 K. To the above solution, 0.06 mole of citric acid in 20 ml of deionized water was added in dropwise, followed by 0.1 mole urea with continuous stirring. In the process, citric acid was employed as a chelating agent, and it facilitated the mixing of cations at the molecular level. The addition of urea to citric acid played a vital role in the formation of tridentated com-

plexes between the metallic cations and citric acid that facilitated the formation of homogeneous, nano-sized particles. The resultant transparent dark bluish solution was heated gently at 363 K with continuous stirring for 6 h to remove the excess water. The solution turned into a transparent dark bluish sol and was allowed to form a polymeric gel, which was heated at 393 K in an oven for 24 h. The dried polymeric precursor was heated at a ramping rate of 4 K min^{-1} and maintained at 423 K for 3 h and 573 K for 3 h, with intermediate grinding. A dark brown $LiCoVO_4$ powder (product A) was obtained after further heating at 773 K for 5 h in air.

Synthesis of La_2O_3-coated $LiCoVO_4$

A polymeric process was employed to prepare the 0.1, 0.5, and 1.0 wt % of La_2O_3-coated $LiCoVO_4$ cathode particles. Chemicals used were $LiCoVO_4$ powders prepared by the polymeric method in the previous section 2.1, $La(NO_3)_3 \cdot 6H_2O$ (Aldrich) and polyvinyl alcohol (PVA, degree of polymerization is 1500). Freshly prepared $LiCoVO_4$ (product A) was dispersed in deionized water by a 1 h sonication, followed by 3 h stirring. The calculated 0.1, 0.5, and 1.0 wt % of $La(NO_3)_3 \cdot 6H_2O$ to form La_2O_3 and PVA were dissolved in warm deionized water and added dropwise to the dispersed $LiCoVO_4$ solution after sonication for 0.5 h. The mixture was stirred for 6 h at 298 K and heated at 363 K with continuous stirring. After removal of excess water for 7–8 h, a thick polymeric gel was formed. The gel was further dried in an oven at 393 K for 12 h to form a dry brown powder, which was heated at 873 K for 2 h in air with a heating ramp rate of 4 K min^{-1} to form a thin layer of La_2O_3 coating on the $LiCoVO_4$ cathode particles (product B) with the weight ratios of 99.9:0.1, 99.5:0.5, and 99.0:1.0, respectively.

Synthesis of La_2O_3-coated $LiCoVO_4$/C composite materials

The La_2O_3-coated $LiCoVO_4$ product (product B) was mixed with malonic acid in acetone, and ball-milled under argon for 30 min. The mixture was then calcined at 873 K for 10 h under a purified atmosphere (5 % H_2 in Ar) and a black powder (product C) was obtained for La_2O_3-coated $LiCoVO_4$/C composite material.

Product characterization

A powder X-ray diffractometer (PXRD), Siemens D-5000, Mac Science MXP18, equipped with a Ni-filtered Cu-K_α radiation source (λ = 1.5405 Å) was used to study the structure and phase purity. The diffraction patterns were recorded between scattering angles of 15° and 80° in steps of 0.05°. Fourier transform infrared (FTIR) spectra were recorded at 298 K on powdered samples using the KBr wafer technique in a Jasco-410 FTIR instrument. The spectra were recorded with a resolution of 2 cm^{-1} in transmittance mode from 400 to 4000 cm^{-1}, corrected for background. The thermal analysis (TG/DTGA) measurements were carried out on a Perkin-Elmer TGA-7 series thermal analysis system in air at a heating rate of 20 K min^{-1} from 298 K. The surface morphological studies were carried out on a Hitachi model S-3500V scanning electron microscope (SEM). The microstructures of the particles were examined by a JEOL JEM-200FXII transmission electron microscope (TEM) equipped with a LaB_6 gun. The sample for TEM study was prepared by dispersing the cathode powder in ethanol, placing a drop of the clear solution on a carbon-coated copper grid, and subsequent drying. X-ray photon spectroscopy (XPS) and the depth profiles of lanthanum, cobalt, vanadium, and oxygen were recorded by an electron spectroscopy for chemical analysis (ESCA) instrument (VG Scientific ESCALAB 250) with monochromatic Al K_α radiation 1486.6 eV. The survey spectra were scanned in the range 0.00–1400.00 eV binding energy (BE) in 1.00 eV steps.

Carbon content analyses of the products were investigated on an OIA Model 1010 TOC Analyzer with an oxygen gas rate at 200 ml/min and a nitrogen gas rate at 350 ml/min. Raman spectroscopy was

performed on samples of powders using an ISA T64000 double beam pass spectrometer equipped with a microscope stage for analyzing small samples utilizing 180° incident geometry. A Spectra Physics argon-ion laser was employed to excite laser Raman spectra using a 515-nm laser line at an incident power of ca. 10 mW along with a water-cooled photomultiplier tube. The scanning rate used to collect the spectra was kept at 10 cm^{-1} min^{-1}. The electronic conductivity of samples was measured by four-point conductivity measurements of Keithley Model 2400S source meter.

The cathodes for electrochemical studies were prepared by a doctor-blade coating method with a slurry of 85 wt % coated active material, 10 wt % conductive carbon black, and 5 wt % poly(vinylidene fluoride) as a binder, in *N*-methyl-2-pyrrolidone (NMP), as the solvent for the mixture, which was then applied onto a surface-cleaned aluminum foil current collector and dried at 393 K for 12 h in an oven. The coated cathode foil was then smoothed by pressing it through stainless-steel twin rollers and cut into circular disks 13 mm in diameter.

The electrochemical performance of the above discs was carried out with coin-type cells of the 2032 configuration and were assembled in an argon-filled VAC MO40-1 glove box in which the oxygen and water contents were maintained below 2 ppm. The above-prepared circular disk was used as the cathode, Li metal (Foote Mineral) as the anode and a 1 M $LiPF_6$ in 1:1 by volume ethylene carbonate (EC)/diethyl carbonate (DEC) (Tomiyama Chemicals) as the electrolyte with a Celgard membrane as the separator. The cells charge–discharge cycles were performed at a 0.1 C-rate between 3.0~4.5 V in a multichannel battery tester (Maccor 4000) at 298 K.

RESULTS AND DISCUSSION

X-ray diffraction

Figure 1 shows the XRD patterns for pristine $LiCoVO_4$ heated at 773 K for 5 h, 0.5 wt % La_2O_3-coated $LiCoVO_4$ at 873 K for 2 h, 0.5 wt % La_2O_3-coated $LiCoVO_4$ calcined with 60 wt % malonic acid, and JCPDS #38-1396 of $LiCoVO_4$, respectively. From Fig. 1a, it is observed that a complete crystalline single phase was formed when calcined at 773 K for 5 h in air. The single-phase purity of the synthesized $LiCoVO_4$ compound could be indexed to the $LiCoVO_4$ (JCPDS #38-1396) pattern that belongs to the inverse spinel structure with $Fd\bar{3}m(O_h^7)$ space group symmetry [36]. The characteristic identity of an inverse spinel structure is the ratio of the Bragg peak intensities of (111) and a strong (220) line [1]. The presence of transition-metal atoms on the tetrahedral coordinated 8a site leads to an increase in the (220) intensity at the expense of the (111) peak that conforms to an inverse spinel structure. The samples heated at 773 K showed the peak intensity ratio for $I(220)/I(311)$ Bragg lines as ~0.5, which indicates the high crystalline nature of the powders. The calculated lattice constant a value and the crystal cell volume for the $LiCoVO_4$ sample were 8.252 Å and 561.92 $Å^3$, respectively, and are consistent with the reported pristine $LiCoVO_4$ samples [1]. In Fig. 1b, the observed XRD peak positions remained the same as pristine $LiCoVO_4$ for the 0.5 wt % La_2O_3-coated $LiCoVO_4$ cathode material, and there are no evident secondary-phase peaks corresponding to La_2O_3. This result indicates that the amount of La_2O_3 coating on the core material was very small and did not reveal any corresponding peaks. Figure 1c displays the XRD pattern of 0.5 wt % La_2O_3-coated $LiCoVO_4$/C composite cathode material, which demonstrates that amorphous carbon was coated on the surface of $LiCoVO_4$ particles according to the XRD pattern of amorphous carbon in Fig. 1d.

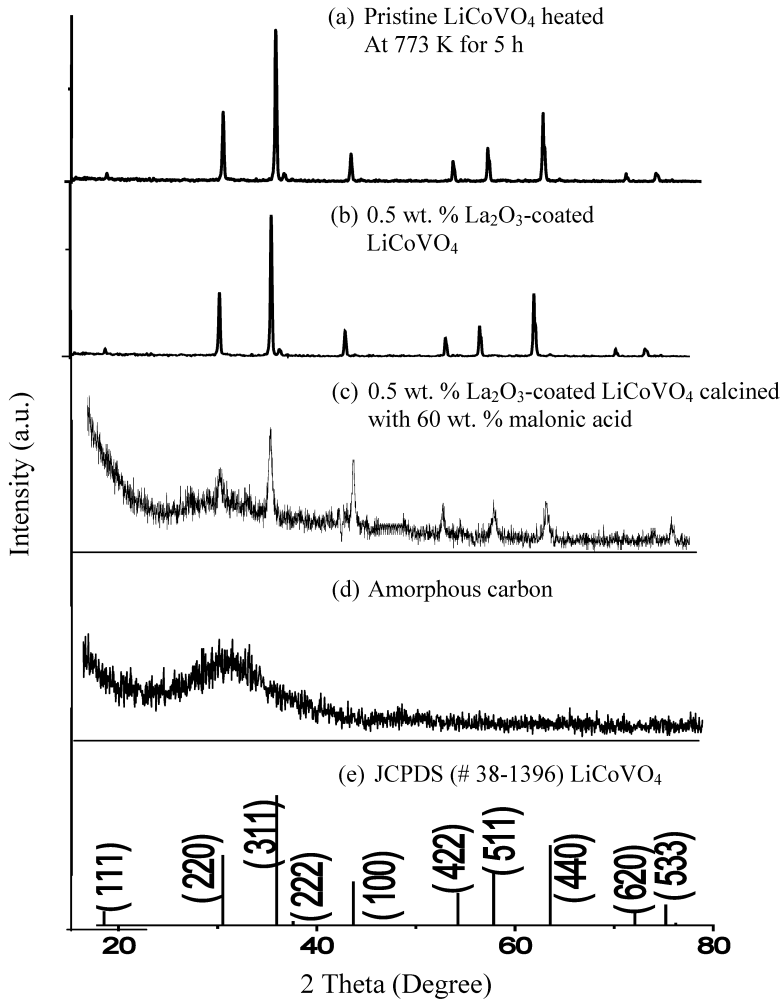

Fig. 1 XRD patterns for (a) pristine $LiCoVO_4$; (b) 0.5 wt % La_2O_3-coated $LiCoVO_4$; (c) 0.5 wt % La_2O_3-coated $LiCoVO_4$ calcined with 60 wt % malonic acid; (d) amorphous carbon; and (e) JCPDS (# 38-1396) $LiCoVO_4$.

TG/DTA analysis

Figure 2 shows the TGA and DTA data curves for the $LiCoVO_4$ polymeric precursor. The TGA curve shows a step-wise weight loss in the temperature ranges 313–423, 423–516, 516–646, and 646–750 K. The initial weight loss of 8 % may correspond to the loss of water and an excess of free citric acid and other organic residues. In the temperature range 423–516 K, the decomposition of the complex into intermediate and the formation of crystalline $LiCoVO_4$ compound, corresponds to the second stage of weight loss and is evidenced by the larger DTA curves. From 516–646 and 646–750 K, complete decomposition of the intermediate occurs and phase-pure $LiCoVO_4$ is formed. The major combustion process was initiated at 423–623 K, and the weight loss slowed down after 750 K. These results were supported by XRD and FTIR results, where the complete formation of crystalline $LiCoVO_4$ at 773 K was confirmed, which agree with the results obtained from the TGA/DTA.

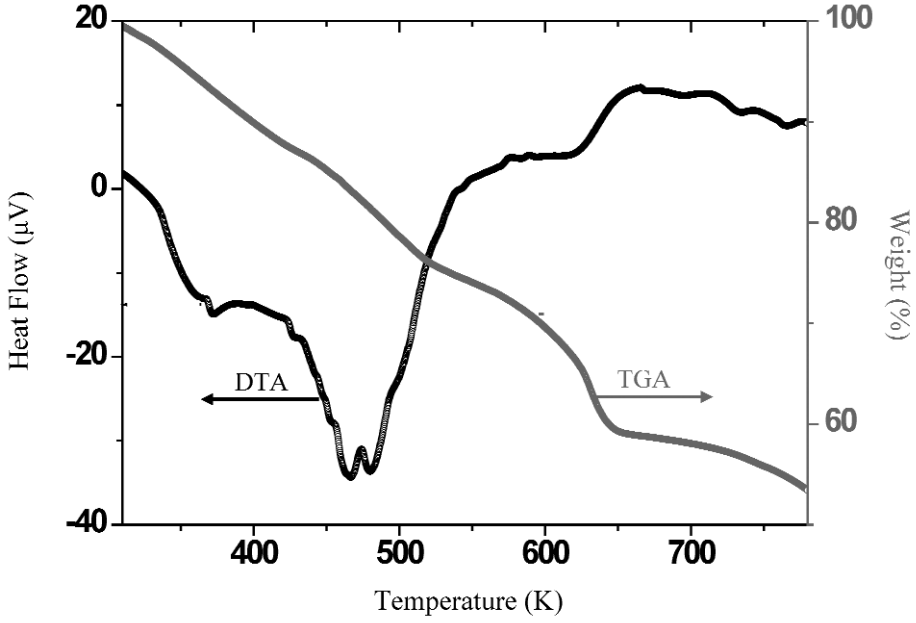

Fig. 2 TG/DTA curves for the as-synthesized pristine $LiCoVO_4$ by a polymeric process.

FTIR analysis

Figure 3 shows the FTIR spectra for $LiCoVO_4$ heated at 393 K for 24 h, 573 K for 3 h, 773 K for 5 h in air and pure $LiCoVO_4$, respectively. In Figs. 3a and 3b, the broad band observed in the region 3200–3600 cm^{-1} is due to the presence of stretching modes of OH groups present in the complexes of citric acid, as well as stretching modes of N–H groups of urea [37]. The low transmittance bands observed at 2858 and 2922 cm^{-1} are attributed to the asymmetric and symmetric stretching of the CH_2 group of the citrate, respectively [37,38]. The FTIR band observed at 1630 cm^{-1} is due to the asymmetric vibrations of carbonyl groups of citric acid and urea with the metal ions [37]. The band observed at 1394 cm^{-1} is due to asymmetric stretching of C–O–C groups as well as the nitrates in the polymeric network. Thus, the FTIR spectra revealed the heat treated samples at 393 and 573 K were formed of metal carboxylate, thereby confirming that the citric acid-urea complex chelates the metal ions. The citric acid functions as a chelating agent that provides a homogeneous distribution of cations such as Li, Co, and V, because these cations are trapped in the citric acid polymeric network. Therefore, it is possible to prepare a very homogeneous oxide powder with nanosized particles. From Fig. 3b, it is observed that the reduction in the intensity of the bands corresponds to the organic residues and appearance of new bands associated with the formation of the $LiCoVO_4$ compound.

In Fig. 3c, the citrate-urea complex bands completely disappeared and formed a crystalline $LiCoVO_4$ compound, when heated at 773 K for 5 h. There is broad strong band in the region of 512–971 cm^{-1} that can be assigned to a stretching vibration between the oxygen and V^{5+} ions of the VO_4 tetrahedron, which has A_1 symmetry and is comprised of sub bands: 733 and 809 cm^{-1}, which agrees with the pure $LiCoVO_4$ shown in Fig. 3d [36]. The broadness of the 512–971 cm^{-1} band could be tentatively explained in terms of the asymmetrical bonding of VO_4 tetrahedron where two types of cations, namely, Li and Co, may be bonded with each oxygen atom of a VO_4 tetrahedron. As a result, asymmetry is introduced to the VO_4 unit without disturbing the overall cubic symmetry of the elementary unit cell.

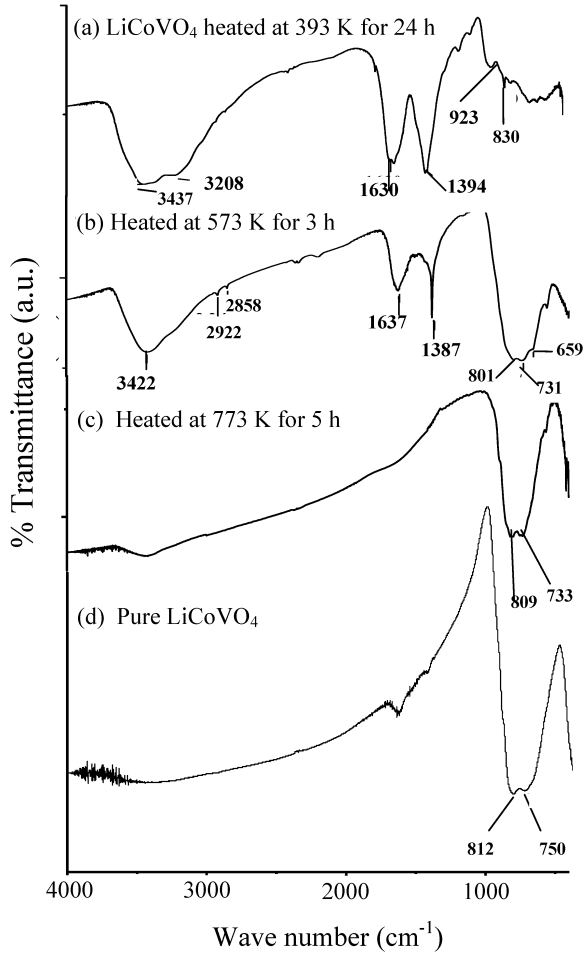

Fig. 3 FTIR spectra for the pristine $LiCoVO_4$ cathode materials heated at (a) 393 K for 24 h; (b) 573 K for 3 h; (c) 773 K for 5 h; and (d) pure $LiCoVO_4$.

Raman, total organic carbon, and conductivity analyses

The structure and conductivity of the deposited carbon on the surface of $LiCoVO_4$ particles were investigated using Raman spectroscopy and four-point dc method, respectively. Micro laser Raman spectroscopy is known to be a useful technique for detecting carbon coating at the surface of coated particles, since the penetration depth of the light inside the particles in Raman scattering is very small. Figure 4 and Table 1 display the Raman spectra of the composite materials in the range of 800~1800 cm^{-1}. The broad bands at 1350 and 1590 cm^{-1} are well known from the spectroscopy of carbon as being the D and G bands that originate from amorphous and graphitic forms, respectively [39,40]. The bands at 1350 and 1590 cm^{-1} can be assigned to the sp^2 graphite-like structure, and the others to the sp^3 amorphous carbonaceous materials [41]. The two strong peaks due to sp^2 and sp^3 carbon bonding in the Raman spectra clearly confirm the presence of carbon coating at the surface of $LiCoVO_4$ particles. The peak intensity ratios between 1350 and 1590 cm^{-1} can be calculated as *R*-values (I_D/I_G), and used to estimate the degree of disordering. This value indicates that the carbon can be pyrolyzed to form highly graphitized carbons with low I_D/I_G ratios and good electronic properties [41].

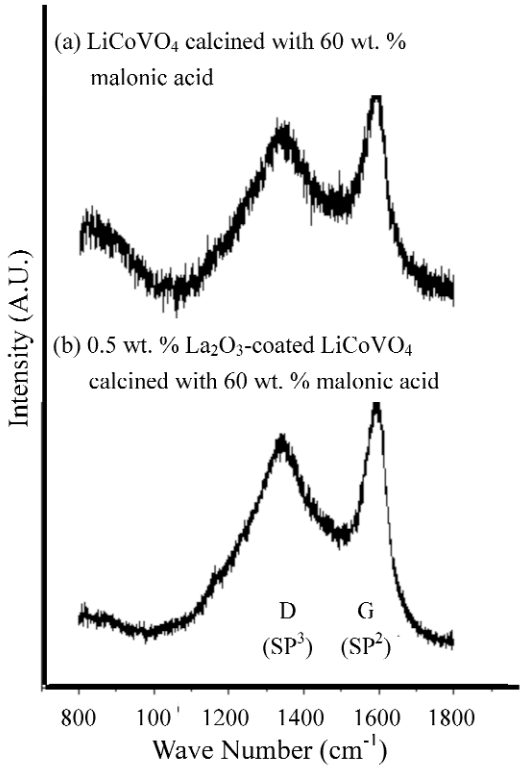

Fig. 4 Raman spectra for (a) $LiCoVO_4$ calcined with 60 wt % malonic acid and (b) 0.5 wt % La_2O_3-coated $LiCoVO_4$ calcined with 60 wt % malonic acid.

Table 1 Comparison of conductivity, carbon content, and I_D/I_G ratios of materials.

Term	Conductivity (S cm^{-1})	TOC (wt %)	Raman		
			Peak (cm^{-1})	Intensity (A.U.)	I_D/I_G ratio
$LiCoVO_4$	8.44×10^{-9}	0	–	–	–
			–	–	
$LiCoVO_4$ calcined with 60 wt % malonic acid	4.88×10^{-4}	2.89	SP^3	1280	0.977
			SP^2	1310	
0.5 wt % La_2O_3-coated $LiCoVO_4$ calcined with 60 wt % malonic acid	9.62×10^{-4}	3.41	SP^3	1370	0.853
			SP^2	1607	

The carbon content was determined by total organic carbon (TOC) analysis. The carbon coating treatment of La_2O_3-coated $LiCoVO_4$ particles with malonic acid greatly improved the electronic conductivity of $LiCoVO_4$ by a factor of five, as shown in Table 1. Conductivity increased along with the carbon content of composite samples that was between 2.8 and 3.5 wt %. The individual $LiCoVO_4$ crystals were wired together by the coated carbon layer, so the carbon layer provides a conductivity network and might increase the conductivity of the materials, which would be beneficial to electrochemical properties.

Electron spectroscopy for chemical analysis

X-ray photoelectron spectroscopy (XPS) has been used widely to study the surface composition and to determine whether the La_2O_3 coating remained on the surface of the core materials or formed a solid solution. Figure 5 shows the XPS spectrum of La 3d at a surface depth of 0 and 30 nm, respectively, for La_2O_3-coated $LiCoVO_4$. From Fig. 5, the La spectrum displays characteristic BEs of 832 eV (La $3d_{5/2}$) and 858 eV (La $3d_{3/2}$) at a surface level, but at a depth of 30 nm, the same peaks were found to be very shallow. The BE values are in agreement with La 3d in La_2O_3 [42]. The difference in peak intensities demonstrates that the La_2O_3 remained on the surface of the core material and did not react to form any solid solution with the pristine material, as supported by our XRD results. As the depth increased, it is clearly noticeable that there was a decrease in La_2O_3 concentration.

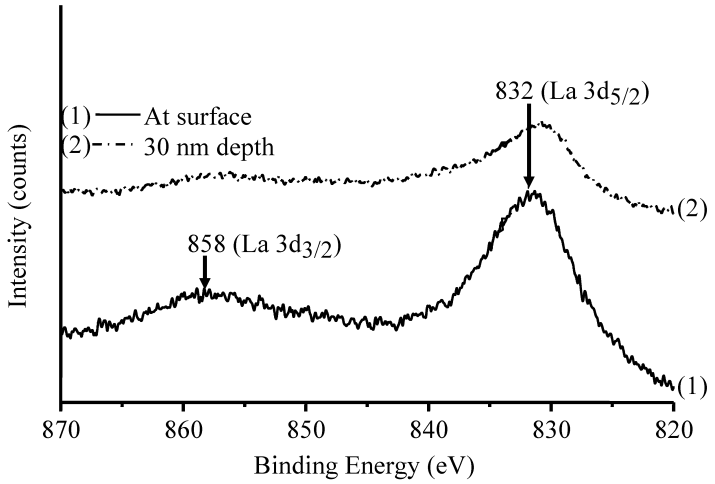

Fig. 5 XPS spectra La 3d of a 0.5 wt % La_2O_3-coated $LiCoVO_4$ particle.

Figure 6 shows the entire spatial distribution of O, Co, V, and La atomic concentrations in La_2O_3-coated $LiCoVO_4$ with a depth profile of the particle up to 100 nm. The concentration of cobalt increased to a depth of about 10 nm and then leveled off. Similarly, the concentration of vanadium increased to a depth of about 20 nm and then leveled off. The high atomic concentration of oxygen at the surface of the oxide is reasonable due to the presence of La_2O_3 oxygen content. The concentration of lanthanum was low, typically less than the 10 at % at the surface level. Beyond that, there was a rapid decrease in the lanthanum concentration with the depth of the particle. The depth profile value corresponds approximately to the thickness 15 nm of the compact layer observed with a TEM image.

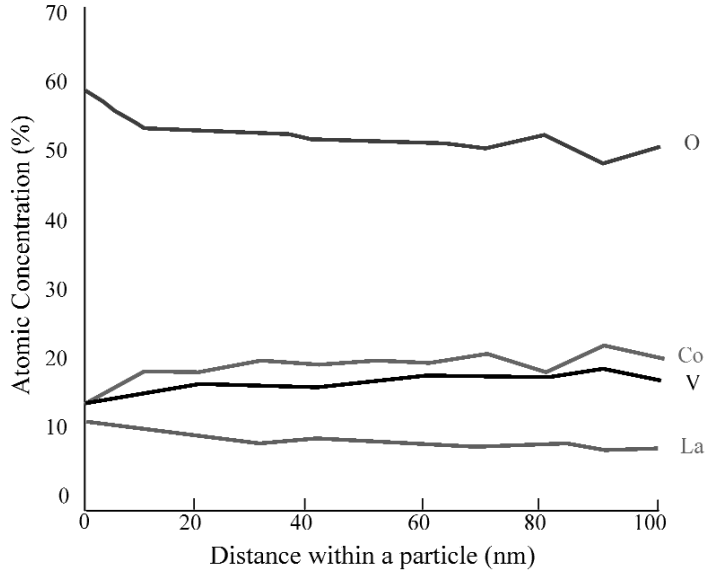

Fig. 6 Depth profile of a 0.5 wt % La_2O_3-coated $LiCoVO_4$ particle.

Morphology

Figure 7 represents the SEM micrographs for the $LiCoVO_4$ cathode material heated at 423 K for 3 h, 573 K for 3 h, and 0.5 wt % La_2O_3-coated $LiCoVO_4$/carbon, respectively. From Fig. 7a, it is observed that the morphology of the sample heated at 423 K contained large particles that had sharp edges. At 573 K in Fig. 7b, these large particles started to break up into flaky structures, due to the decomposition of the citric-urea complexes, as is also evident in the TGA results. From Fig. 7c, the individual $LiCoVO_4$ crystals were wired together by the coated carbon layer, so they aggregated to form the grains several hundred micrometers in size.

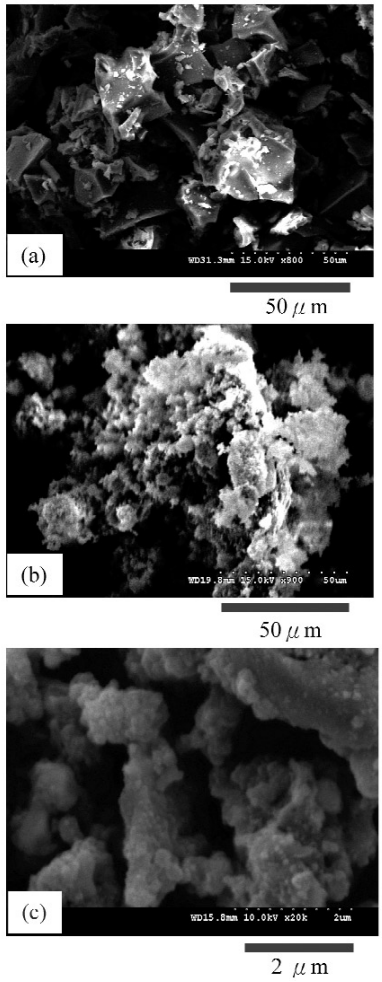

Fig. 7 SEM micrographs of the $LiCoVO_4$ powders prepared by a citric acid-urea process at different temperatures: (a) 423 K for 3 h; (b) 573 K for 3 h; and (c) 0.5 wt % La_2O_3-coated $LiCoVO_4$ calcined with 60 wt % malonic acid.

In order to observe the microstructure of $LiCoVO_4$ and related coated materials, we studied those powders further using TEM/energy-dispersive spectrometry (EDS)/ selected area electron diffraction (SAED) methods. Figures 8a, 8b, and 8c show the TEM images of the pristine $LiCoVO_4$, the 0.5 wt % La_2O_3-coated $LiCoVO_4$, and 0.5 wt % La_2O_3-coated $LiCoVO_4$/C composite materials, respectively. In Fig. 8a, it is evident that $LiCoVO_4$ crystallines are uniform spherical nanosized particles with better dispersion and the average size of these unique nanosized particles ranges from 90 to 100 nm. The particles shown in Fig. 8a have a unique nanosized spherical shape, which can be attributed to the action of the chelating agent assisted with urea that prevents phase separation and leads to the formation of unidentated complexes between the metallic cations and citric acid that facilitates the formation of homogeneous and nanosized particles. In Fig. 8b, there is a thin layer on the surface of the core material in the form of a blanket that had a thickness of about 15 nm. The surface composition was identified as La_2O_3 by the EDS data of Fig. 8d. It is suggested that La_2O_3 is a good additive and can provide enough adherent interaction between the core and the coating materials. The dark areas in Figs. 8b and 8c exhibit a crystalline pattern in either Figs. 8i or 8k, which was identified as $LiCoVO_4$ based on the EDS results of Figs. 8e and 8g. As for Fig. 8c, the TEM image of 0.5 wt % La_2O_3-coated $LiCoVO_4$ cal-

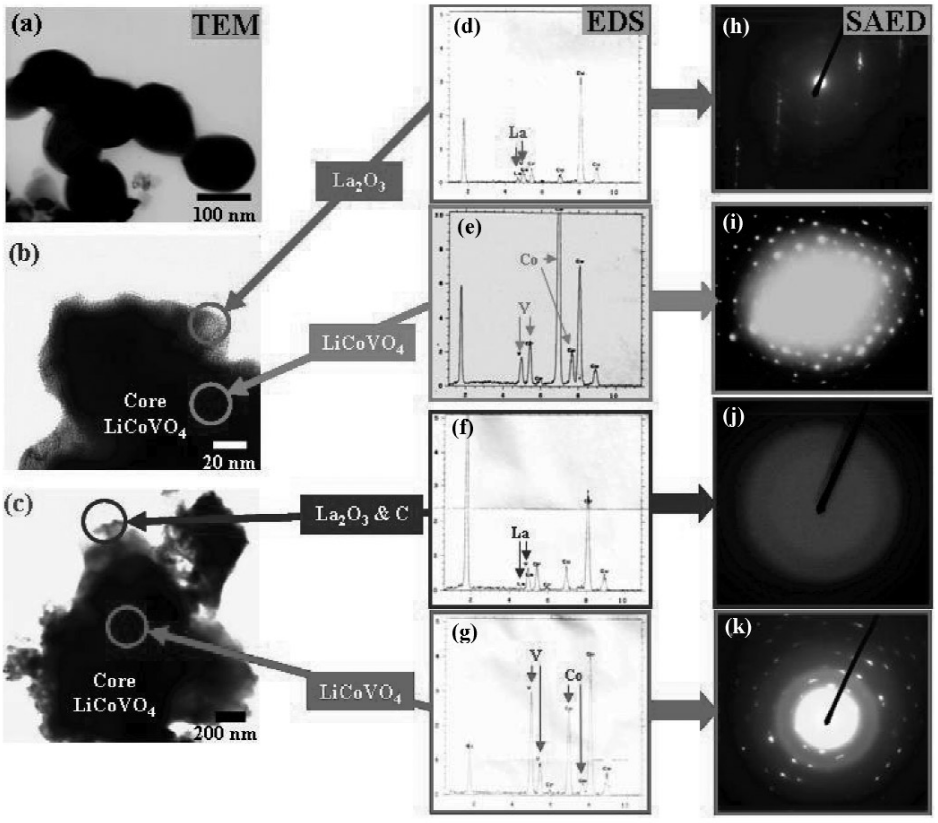

Fig. 8 TEM images of (a) pristine $LiCoVO_4$; (b) 0.5 wt % La_2O_3-coated $LiCoVO_4$; (c) 0.5 wt % La_2O_3-coated $LiCoVO_4$ calcined with 60 wt % malonic acid; (d~g) EDS analysis for the coated materials; (h~k) SAED for the coated materials.

cined with 60 wt % malonic acid is similar to that in Fig. 8b. Unfortunately, no carbon peak was observed in the EDS spectrum in Fig. 8f because our TEM/EDS instrument could not detect any element with an atomic number less than 16. Therefore, carbon and oxygen could not be determined. However, the presence of amorphous carbon can be confirmed by the appearance of hollow ring patterns in SAED in Figs. 8j and 8k.

Differential scanning calorimetry analysis

Figure 9 shows the differential scanning calorimetry (DSC) curves for the bare or pristine $LiCoVO_4$, 0.5 wt % La_2O_3-coated $LiCoVO_4$, 60 wt % malonic acid-coated $LiCoVO_4$, and 0.5 wt % La_2O_3-coated $LiCoVO_4$ calcined with 60 wt % malonic acid cathode material, charged to 4.5 V at a 0.1 C-rate and then potentiostatted at 4.5 V vs. Li^+ for 10 h. In Fig. 9, the bare cathode material displays two characteristic exothermic peaks with major decomposition temperature at 453 K and a minor one at 522 K. All three coated cathode materials exhibit a single exothermic peak with a shift toward a higher decomposition temperature by 7–23 K. The onset temperature of the thermal decomposition was raised significantly, and the total reaction heat was reduced greatly by La_2O_3 and/or malonic acid-coatings, as shown in Fig. 9. The DSC results show that the 0.5 wt % La_2O_3-coated $LiCoVO_4$ sample calcined with 60 wt % malonic acid demonstrated the best thermal stability of the materials we studied. The heat evolution due to the bare cathode material was 176 Jg^{-1}, while the heat evolution due to the La_2O_3-coated

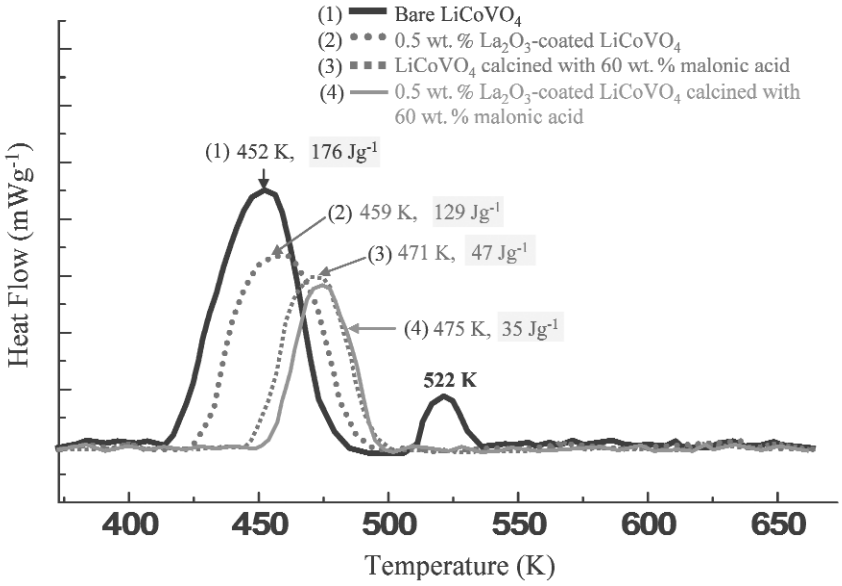

Fig. 9 DSC curves of different cathode materials after full charge at 4.5 V vs. Li for 10 h.

$LiCoVO_4$/C composite cathode material was greatly reduced to 35 Jg^{-1}. The decreased heat evolution is substantiated by literature reports on coated samples compared with uncoated samples [43–46]. Hence, La_2O_3 and malonic acid-coated $LiCoVO_4$ significantly depressed exothermic activity and reduced heat generation at a highly delithiated state.

Galvanostatic cycling behavior

The galvanostatic cycling behavior of 0.1, 0.5, and 1.0 wt % La_2O_3-coated $LiCoVO_4$ is compared with that of pristine $LiCoVO_4$ prepared by a citric acid-urea polymeric method. Figure 10 shows the discharge curves of pristine $LiCoVO_4$ and 0.1, 0.5, and 1.0 wt % La_2O_3-coated $LiCoVO_4$ and 0.5 wt % La_2O_3-coated $LiCoVO_4$ calcined with malonic acid. The initial charge–discharge capacity of pristine $LiCoVO_4$ was 71 and 61 $mAhg^{-1}$, respectively. After 10 cycles, the discharge capacity was 33 $mAhg^{-1}$ and cycling efficiency 54 % for the first 10 cycles. Furthermore, its capacity fading increased with continuous cycling and dropped to 10 $mAhg^{-1}$ at 30 cycles. On the other hand, the discharge capacities and cycle stability were enhanced for the La_2O_3-coated cathode materials, compared to the pristine cathode. The initial discharge capacities of 0.1, 0.5, and 1.0 wt % La_2O_3-coated $LiCoVO_4$ were 57, 54, and 58 $mAhg^{-1}$, respectively. After 30 cycles, the discharge capacities of the 0.1, 0.5, and 1.0 wt % La_2O_3-coated samples were 29, 38, and 33 $mAhg^{-1}$ and cycling efficiency 50, 70, and 57 % for the first 30 cycles, respectively.

In Fig. 10, the La_2O_3-coated samples also had an initial drastic fall in capacity for the first 15 cycles, but thereafter, it retained good cycle stability for about 110 cycles. Compared to various wt % coating levels, the 0.5 wt % La_2O_3-coated sample exhibited the best discharge capacity and cycle stability. As a result of the La_2O_3 coating, the cathode material was protected from direct contact with the HF-containing electrolyte. Furthermore, the cell capacity and cycle life improved significantly after malonic acid treatment. For instance, a 0.5 wt % La_2O_3-coated $LiCoVO_4$ sample calcined with 60 wt % malonic acid can provide an initial capacity of 71 $mAhg^{-1}$ and reach 60 $mAhg^{-1}$ at 30 cycles.

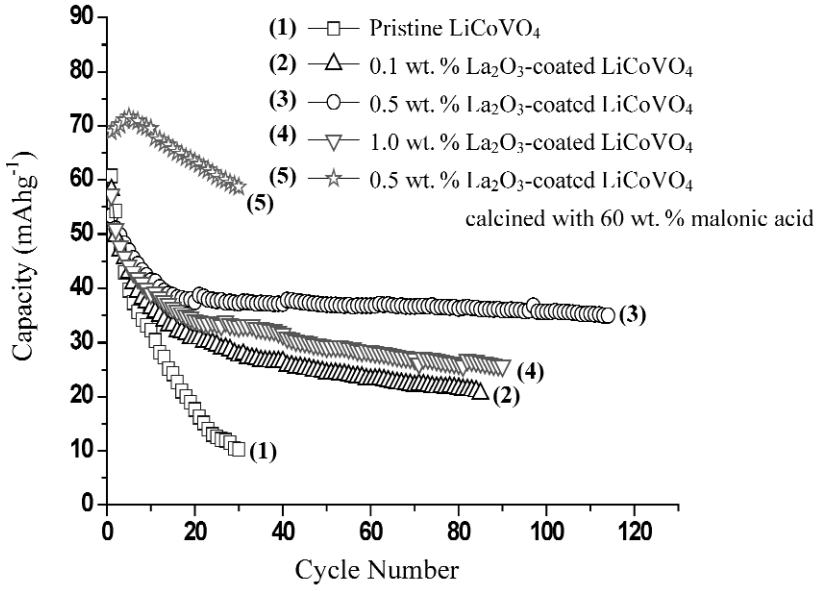

Fig. 10 Discharge curves of the pristine $LiCoVO_4$ and the coated cathode materials. Charge–discharge: 0.1 C-rate between 3.0 and 4.5 V.

CONCLUSIONS

A citric acid-urea polymeric method was successfully applied to synthesize nanocrystalline $LiCoVO_4$ cathode materials. Pure-phase inverse spinel $LiCoVO_4$ powders with average particle sizes of about 95 nm were easily prepared at 773 K for 5 h in air. Raman and XPS analyses confirmed the presence of carbon and La_2O_3 coating on the surface of $LiCoVO_4$ powders. The surface of the $LiCoVO_4$ cathode was coated with various wt % of La_2O_3 by a polymeric process. XRD results revealed that complete crystallization occurred at a low temperature of 773 K for 5 h. FTIR spectral results confirmed the complete removal of organic residues at a low temperature and the formation of $LiCoVO_4$. SEM micrographs showed the morphology of the materials at different stages of the synthesized compound. TEM images revealed that the particles were a uniform nanosize of about 95 nm and the coated layer was about 15 nm thick on the $LiCoVO_4$ material. The electrochemical performance of the Li/$LiCoVO_4$ cell demonstrated good capacity retention when charged to a high voltage of 4.5 V. The cell performance of pristine $LiCoVO_4$ synthesized by a citric acid-urea process sustained 10 $mAhg^{-1}$ for 30 cycles and 0.5 wt % La_2O_3-coated $LiCoVO_4$ sustained 37 $mAhg^{-1}$ for 110 cycles. However, the sample obtained from a 0.5 wt % La_2O_3-coated $LiCoVO_4$ calcined with 60 wt % malonic acid demonstrated the best cell performance and thermal stability of the materials we studied. It had an initial capacity of 71 $mAhg^{-1}$ and reached 60 $mAhg^{-1}$ at 30 cycles. The onset temperature of thermal decomposition of this composite cathode material was 475 K compared to 452 K for bare $LiCoVO_4$. The total reaction heat was reduced significantly by La_2O_3 and malonic acid coatings and its heat evolution was 35 Jg^{-1} vs. 176 Jg^{-1} for bare $LiCoVO_4$, after they were charged to 4.5 V at a 0.1 C-rate and then potentiostatted at 4.5 V vs. Li^+ for 10 h. These results demonstrate a remarkable improvement of the $LiCoVO_4$ cathode material in terms of capacity, cycle life, and thermal stability.

ACKNOWLEDGMENTS

Financial support for this work was provided by the National Science Council of the Republic of China under contract No. NSC 93-2214-E-008-004. PMD thanks the NSC for the award of a postdoctoral fellowship.

REFERENCES

1. G. T. K. Fey, W. Li, J. R. Dahn. *J. Electrochem. Soc.* **141**, 227 (1994).
2. G. T. K. Fey. *J. Active Passive Electronic Components* **18**, 11 (1995).
3. G. T. K. Fey, W. B. Perng. *Mater. Chem. Phys.* **47**, 279 (1997).
4. G. T. K. Fey, K. S. Wang, S. M. Yang. *J. Power Sources* **68**, 159 (1997).
5. G. T. K. Fey, J. R. Dahn, M. J. Zhang. W. Li. *J. Power Sources* **68**, 549 (1997).
6. G. T. K. Fey, C. S. Wu. *Pure Appl. Chem.* **69**, 2329 (1997).
7. G. T. K. Fey, K. S. Chen. *J. Power Sources* **81/82**, 467 (1999).
8. C. H. Lu, W. C. Lee, S. J. Liou, G. T. K. Fey. *J. Power Sources* **81/82**, 696 (1999).
9. G. T. K. Fey, D. L. Huang. *Electrochim. Acta* **45**, 295 (1999).
10. P. P. Chu, D. L. Huang, G. T. K. Fey. *J. Power Sources* **90**, 95 (2000).
11. B. J. Hwang, Y. W. Tsai, G. T. K. Fey, J. F. Lee. *J. Power Sources* **97/98**, 551 (2001).
12. S. R. S. Prabaharan, M. S. Michael, S. Radhakrishna, C. Julien. *J. Mater. Chem.* **7**, 1791 (1997).
13. J. R. Liu, M. Wang, X. Lin, D. C. Yin, W. D. Huang. *J. Power Sources* **108**, 113 (2002).
14. P. Kalyani, N. Kalaiselvi, N. Muniyandi. *Mater. Chem. Phys.* **77**, 662 (2002).
15. S. Vivekanandhan, M. Venkateswarlu, N. Satyanarayana. *Mater. Lett.* **58**, 1218 (2004).
16. T. Thongtem, A. Phuruangrat, S. Thongtem. *Mater. Lett.* **60**, 3776 (2006).
17. N. V. Landschoot, E. M. Kelder, P. J. Kooyman, C. Kwakernaak, J. Schoonman. *J. Power Sources* **138**, 262 (2004).
18. G. T. K. Fey, P. Muralidharan, Y. D. Cho. *J. Power Sources* **174**, 1152 (2007).
19. G. T. K. Fey, P. Muralidharan, C. Z. Lu, Y. D. Cho. *Solid State Ionics* **177**, 877 (2006).
20. G. G. Amatucci, J. M. Tarascon, L. C. Klein. *Solid State Ionics* **83**, 167 (1996).
21. S. T. Myung, K. Izumi, S. Komaba, Y. K. Sun, H. Yashiro, N. Kumagai. *Chem. Mater.* **17**, 3695 (2005).
22. H. Wang, Y. I. Jang, B. Huang, D. R. Sadoway, Y. M. Chiang. *J. Electrochem. Soc.* **146**, 473 (1999).
23. L. F. Wang, C. C. Ou, K. A. Striebel, J. S. Chen. *J. Electrochem. Soc.* **150**, A905 (2003).
24. K. M. Shaju, G. V. Subba Rao, B. V. R. Chowdari. *Electrochim. Acta* **48**, 145 (2002).
25. G. H. Kim, S. T. Myung, H. J. Bang, J. Prakash, Y. K. Sun. *Electrochem. Solid-State Lett*. **7**, A477 (2004).
26. D. Zane, M. Carewska, S. Scaccia, F. Cardellini, P. P. Prosini. *Electrochim. Acta* **49**, 4259 (2004).
27. K. Konstantinov, S. Bewlay, G. X. Wang, M. Lindsay, J. Z. Wang, H. K. Liu, S. X. Dou, J. H. Ahn. *Electrochim. Acta* **50**, 421 (2004).
28. M. Gabersceka, R. Dominkoa, M. Belea, M. Remskarb, D. Hanzelb, J. Jamnika. *Solid State Ionics* **176**, 1801 (2005).
29. M. R. Yang, T. H. Teng, S. H. Wu. *J. Power Sources* **159**, 307 (2006).
30. T. Nakamura, Y. Miwa, M. Tabuchi, Y. Yamada. *J. Electrochem. Soc.* **153**, A1108 (2006).
31. P. S. Herle, B. Ellis, N. Coombs, L. F. Nazar. *Nat. Mater.* **3**, 147 (2004).
32. S. Y. Chung, J. T. Blocking, Y. M. Chiang. *Nat. Mater.* **2**, 123 (2002).
33. J. F. Ni, H. H. Zhou, J. T. Chen, X. X. Zhang. *Mater. Lett.* **59**, 2361 (2005).
34. M. Abbate, S. M. Lala, L. A. Montoro, J. M. Rosolen. *Electrochem. Solid-State Lett.* **8**, A288 (2005).

35. G. X. Wang, S. Bewlay, J. Yao, J. H. Ahn, S. X. Dou, H. K. Liu. *Electrochem. Solid-State Lett.* **7**, A503 (2004).
36. C. Julien, M. Massot, C. Pérez-Vicente. *Mater. Sci. Eng. B* **75**, 6 (2000).
37. W. Kemp. *Organic Spectroscopy*, Palgrave, New York (2002).
38. Y. M. Hon, K. Z. Fung, S. P. Lin, M. H. Hon. *J. Solid State Chem.* **163**, 231 (2002).
39. M. M. Doeff, Y. Hu, F. McLarnon, R. Kostecki. *Electrochem Solid-State Lett.* **6**, A207 (2003).
40. Y. Hu, M. M. Doeff, R. Kostecki, R. Finones. *J. Electrochem. Soc.* **151**, A1279 (2004).
41. M. M. Doeff, Y. Hu, F. McLarnon, R. Kostecki. *Electrochem. Solid-State Lett.* **6**, A207 (2003).
42. <http://www.xpsdata.com/>: Fundamental XPS data from pure elements, pure oxides, and chemical compounds.
43. D. D. MacNeil, Z. Lu, Z. Chen, J. R. Dahn. *J. Power Sources* **108**, 8 (2002).
44. Y. Baba, S. Okada, J.-I. Yamaki. *Solid State Ionics* **148**, 311 (2002).
45. J. Cho. *Electrochem. Commun.* **5**, 146 (2003).
46. G. T. K. Fey, P. Muralidharan, C. Z. Lu, Y. D. Cho. *Electrochim. Acta* **51**, 4850 (2006).